UDEC Simulation of Triaxial Testing of Lithophysal Tuff

M.C. Christianson
Itasca Consulting Group, Inc., Minneapolis, Minnesota, USA

M.P. Board & D.B. Rigby
Bechtel SAIC LLC, Las Vegas, Nevada, USA

ABSTRACT: The current conceptual design for the proposed nuclear waste repository at Yucca Mountain Nevada includes placing most of the facility in lithophysal Tuff. Because it is difficult to conduct standard confined triaxial laboratory tests on lithophysal tuff, it was decided to use *UDEC* to conduct numerical triaxial testing of simulated lithophysal tuff samples to supplement existing uniaxial compression data. The results of these numerical experiments are intended to provide guidance on the variability of physical properties as a function of lithophysal porosity. These data can then be used as a basis for large scale modeling of the behavior of the repository drifts. The results of the numerical testing were encouraging and show consistent trends in tuff strength and overall performance as a function of lithophysal porosity.

1.0 INTRODUCTION

The repository horizon for the proposed nuclear spent-fuel waste repository at Yucca Mountain Nevada is located in both lithophysal and nonlithophysal rock units in the Topopah Spring Tuff. The nonlithophysal rocks are characterized as hard, strong, jointed. The lithophysal rocks typically contain about 20 to 30 percent cavities, are more deformable, and have a lower uniaxial compressive strength (UCS). The lithophysae vary in size from a few centimeters to more than 1 meter in diameter. For this paper, lithophysal porosity is defined to be the ratio of volume of lithophysal voids to total sample volume.

Normal testing procedures recommend that the test sample dimension should be at least 10 times the size of any mineral grains or other inclusions. The void size would dictate that very large samples would need to be tested. The representative elementary volume of lithophysal rock is of the order of cubic meters to cubic decameters, depending on the size of lithophysae. In order to develop an adequate correlation between lithophysal porosity and mechanical properties of lithophysal rock, sufficient numbers of laboratory tests on large-size rock samples were desired. However, as a consequence of the size of rock samples required, the lack of high-capacity equipment needed to test such large samples and the cost and time that would be required to produce an adequate statistical database, a suitable laboratory testing effort was impractical to carry out. The presence of voids intersecting the sample surface also makes standard triaxial testing difficult or impossible.

It is apparent that the uniqueness of lithophysal rock poses formidable challenges to obtaining data directly by the process of testing larger rock specimens. The problem, therefore, is how to characterize the uncertainty and spatial variability of the mechanical properties of this material.

To overcome the inability to conduct adequate physical testing, a numerical approach was used to supplement the existing intact rock property database and to confirm the mechanical property estimates of lithophysal rock. This paper presents a systematic method of creating a numerical model of the material, calibrating that model against existing data, and then conducting numerical triaxial tests to supplement existing data. These supplemental data can then be used to predict the larger scale behavior of the repository.

2.0 *UDEC* MODEL

The *UDEC* program is used to generate a 1 m × 1 m rock "sample" composed of a large number of random, irregular, and interconnected blocks or "grains" with average dimension of 0.017 m. It is important that the sample contain blocks that are sufficiently small that they do not dictate where and how fractures can form and propagate. The blocks in the model are defined by randomized Voronoi tessellation that is controlled by supplying a Voronoi seed value. Voronoi tessellation is a term describing the discretization technique used to construct a material model that is composed of a sufficient number of small blocks to allow a realistic propagation of fractures in the model. A plane strain assumption is used in the modeling so that each simulated rock specimen is considered to have an infinite depth. Figure 1 shows an example of one such model. Several different tessellations were used to ensure that the results were not particular to a specific geometry.

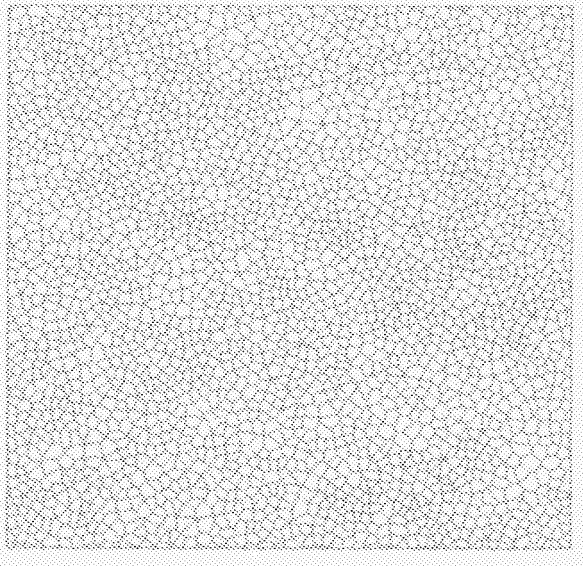

Figure 1 UDEC rock "sample" composed of irregular blocks bonded with frictional and cohesive interfaces

Each block is subdivided into finite difference zones for full deformability of the matrix. The following parameters characterize the mechanical behavior of the *UDEC* Voronoi model (These micro properties are illustrated in Figure 2):

- elastic properties of blocks (E^m, ν^m); and

- properties of joints, both elastic (normal stiffness, k_n, and shear stiffness, k_s) and plastic (tensile strength, t^m, cohesion, c^m, and friction, ϕ^m). The plastic joint parameters are functions of shear and tensile plastic strains. In the simulations presented in this report, it is assumed that cohesion and tensile strength soften to zero at the onset of yield.

3.0 MODEL CALIBRATION

The cohesion and friction angle of the micro-joints are used to control the sample's uniaxial compressive strength. The normal and shear stiffnesses of micro-joints, as well as the bulk and shear moduli of the intact rock (blocks), are used to control the sample modulus.

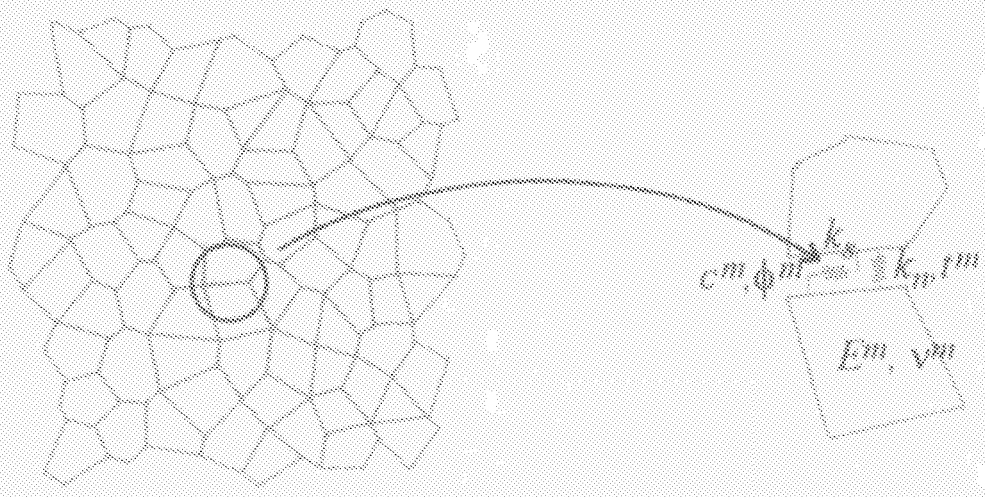

Figure 2 Micro properties of the UDEC *Voronoi Model*

The elastic and strength properties can be decoupled during the iteration process (i.e., model deformability and strength) can be calibrated separately. It is easiest to calibrate model elastic parameters first. Clearly, calibration of the elastic properties is a problem with a non-unique solution. The two elastic macro-properties (E and ν) are functions of block size and four micro properties (k_n, k_s, E^m, and ν^m). The average block size is determined based on having a sufficient number of blocks to allow for consistent and repeatable results in the two-dimensional sample given the sample size and lithophysal void size and shape (e.g., fracture development and propagation is independent of block size and orientation). The Poisson's ratio of the blocks is selected to be equal to the macro Poisson's ratio, such that $\nu^m = \nu$. The additional requirement needed to match the macro Poisson's ratio is that the ratio between normal and shear joint stiffness is greater than 1. Simulations confirmed that a Poisson's ratio of 0.2 is matched when $k_n / k_s \approx 2$. It is desirable, from the perspective of calculation efficiency, that the stiffness of the blocks and the joints are of the same order of magnitude. Therefore, based on information in the *UDEC* User's Guide Manual (Itasca 2002, Problem Solving, Section 3.2.3), it was selected that

$$5 < \frac{K^m + \frac{4}{3} G^m}{b k_s} < 10 \qquad (1)$$

where b is the average block size, and K^m and G^m are the bulk and shear moduli of the blocks, respectively. With these considerations, there is a single independent elastic micro-parameter (e.g. k_n). The proper macro deformability of the model then was matched by rescaling of the elastic micro-properties (k_n, k_s, K^m, and G^m).

Calibration of strength micro-properties involved matching the macro (laboratory scale) failure-envelope and post-peak behavior by adjusting strength micro-properties. The model plastic deformation appears to be a function of the size and shape of blocks. The failure envelope, which, in general, is a surface in the principal stress space, reduces to a line if it is assumed that the failure envelope is not a function of the intermediate principal stress. Test runs have proven that the micro friction angle, which is initially equal to 35° and softens in a brittle fashion to 15°, results in the desired post-peak behavior and strength increase as a function of confinement. In order to match the observed mode of failure for lithophysal tuff with no cavities under uniaxial loading conditions (i.e., axial splitting), the micro tensile strength is assigned to be less than 50 of the micro cohesion. After these relations are established, the proper peak strength is matched by rescaling micro cohesion and tensile strength.

Each sample was tested with a loading condition that simulated either tensile, uniaxial compression (UCS) or triaxial compression (with confinement pressures of 1 MPa, 3MPa, and 5 MPa). The loading of each sample was controlled by a FISH function that adjusts the axial loading velocity to limit the axial stress difference between the top and the bottom of the sample. This ensures that the sample is not loaded faster than the stresses can be transferred numerically through the entire sample.

In all cases, the tests simulated a frictionless platen at the top and bottom of the sample. The axial stresses are generated in response to a controlled velocity condition on the top of the sample. In the case of triaxial compression, a constant lateral confining stress is applied to the sample edges prior to the axial loading of the sample. The applied confining stress does not extend into lithophysal voids that intersect the edges. The lateral confining stresses were adjusted based on the actual loaded surface area to ensure that the total force was equal on both sides of the sample.

The axial stress is defined by the sum of the reaction forces at the loading 'platen' divided by the original sample width. The axial strain is defined as the change in distance between the 'platens' divided by the original sample height. The volumetric strain is calculated by integrating the current sample width over the current sample height and dividing by the original sample volume. These quantities are calculated automatically and recorded at regular intervals during the test.

The target modulus and uniaxial compressive strength were selected to match the lithophysal tuff properties derived in the *PFC* lithophysal study (Potyondy 2002). The values of 20 GPa for Young's modulus and 60 MPa for uniaxial compressive strength were used as the target values for the calibration of large-core lithophysal tuff with zero percent lithophysal porosity. The lithophysal porosity is defined as the lithophysal volume fraction (ratio of volume of inserted voids to total sample volume). There is an inherent matrix porosity included in the numerical rock model, as the calibration is based on intact rock specimens having a matrix groundmass porosity of about 10 percent. The calibration process produced the micro- and fracture

properties given in Table 1. The average values from five model samples (with different Voronoi seeds) were 19.8 GPa and 58.7 MPa for the modulus and UCS, respectively.

Table 1 ***Table 1. Calibrated UDEC (micro) fracture properties to reproduce lithophysal rock with no cavities average intact strength and deformability***

Parameter	Value	Unit
Intact Bulk Modulus	23.0	GPa
Intact Shear Modulus	17.2	GPa
Joint Normal Stiffness	2360.0	GPa/m
Joint Shear Stiffness	1180.0	GPa/m
Joint Cohesion	22.0	MPa
Joint Friction	35.0	Degrees
Joint Tension	9.0	MPa
Residual Cohesion	0.0	MPa
Residual Friction	15.0	Degrees
Residual Tension	0.0	MPa

4.0 LITHOPHYSAL SAMPLES

The generation of the lithophysal samples resulted from cutting 90-mm diameter holes in the non-lithophysal samples. The position of the holes was controlled using one of two techniques. Some of the samples were created to match specific simulated samples used in a previous *PFC* lithophysal study (Potyondy 2002). The rest of the samples were generated using a FISH function with a random number generator that specified the location of the holes. Successive holes are introduced until the total area of the removed material matches the desired lithophysal porosity.

In both techniques, there were some simple rules that were used for the placement of holes. These rules are necessary to ensure that the bridges between voids contain more than one block and to ensure that the collapse of voids does not affect the applied boundary conditions. The first rule is that the distance between the edges of adjacent holes can never be less than 0.041 m. The second rule is that there must be at least a 0.045-m distance between the edge of a hole and the sample sides (unless the hole intersects the side). If the hole intersects the sample side, then the intersection is limited to half the diameter or less.

Several samples were generated for three target nominal lithophysal porosities of 10%, 17% and 24%. In each case, the placement of the holes was varied. Because of the placement rules, it was not possible to generate samples with lithophysal porosities s greater than approximately 26%. Figures 3-5 show typical samples representing each of the lithophysal porosities.

5.0 NUMERICAL SAMPLE TESTS

A series of tensile, uniaxial and triaxial compression numerical experiments were conducted on the lithophysal samples as described above. Figures 6-8 show samples of the stress strain curves from each of the nominal lithophysal porosity groups.

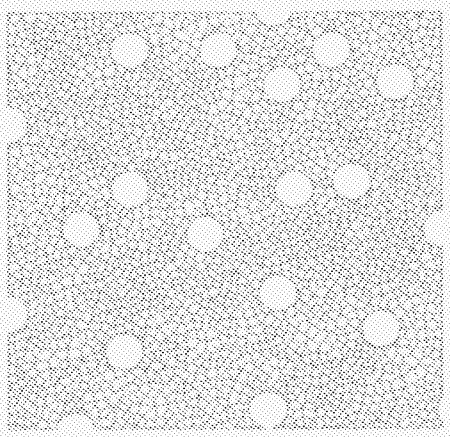

Figure 3 UDEC model with lithophysal porosity of 10%

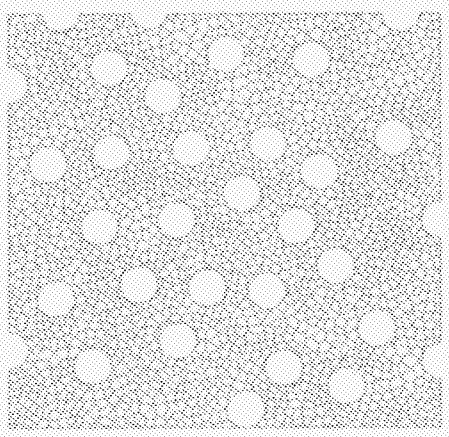

Figure 4 UDEC model with lithophysal porosity of 17%

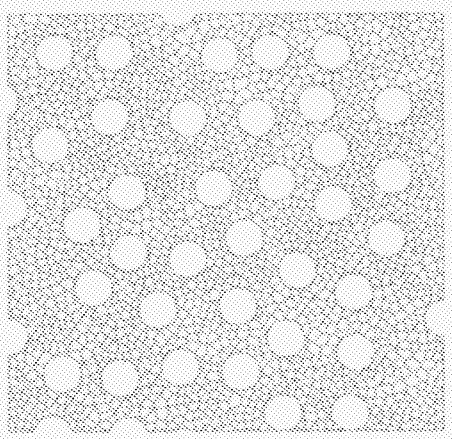

Figure 5 UDEC model with lithophysal porosity of 24%

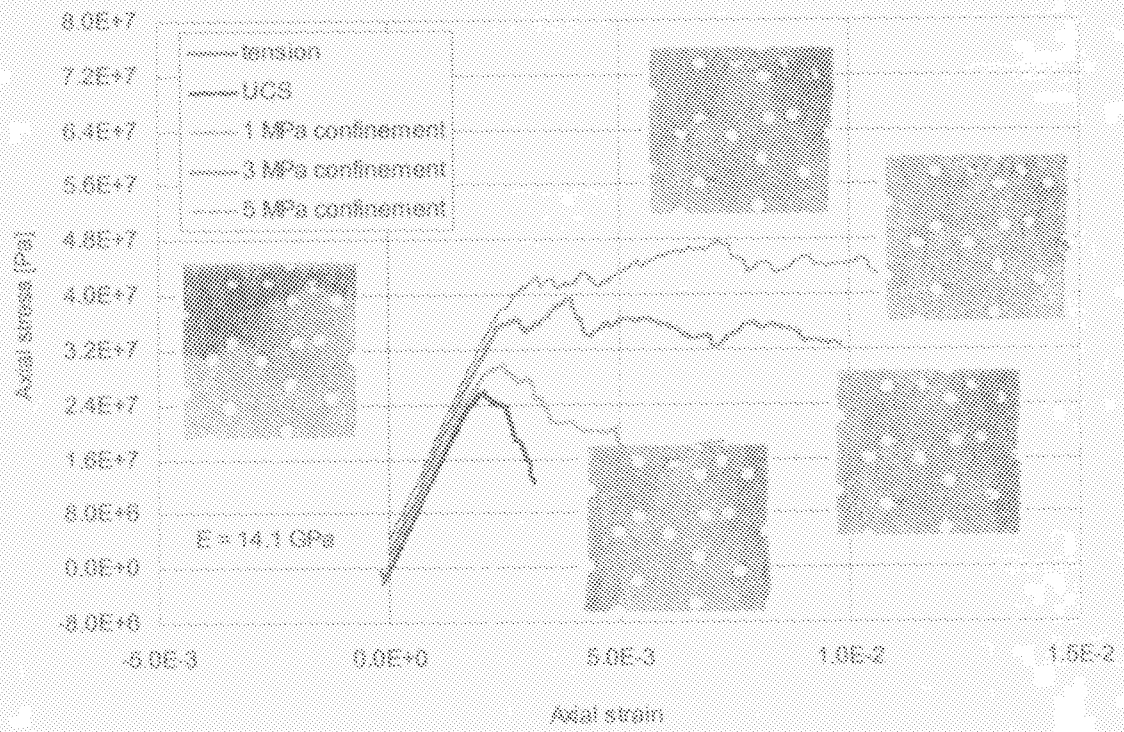

Figure 6 Stress-strain response and failure mechanisms for lithophysal porosity of 10.3% (circular voids distributed randomly throughout the sample)

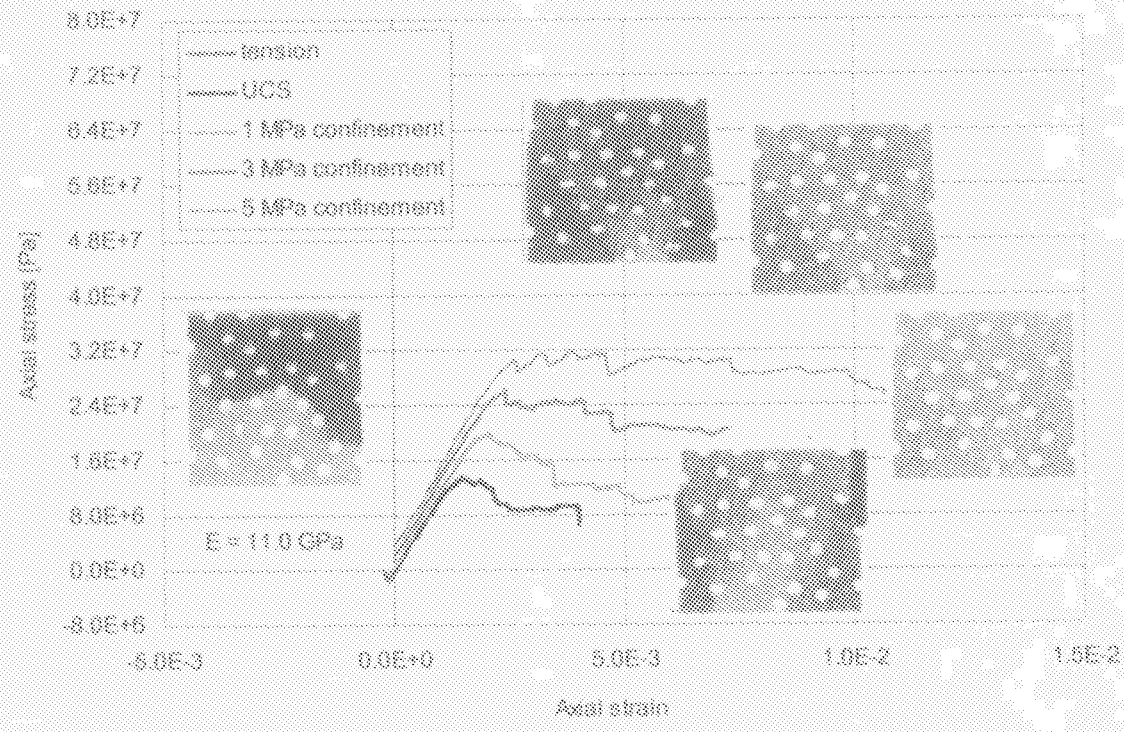

Figure 7 Stress-strain response and failure mechanisms for lithophysal porosity of 17.8% (circular voids distributed randomly throughout the sample)

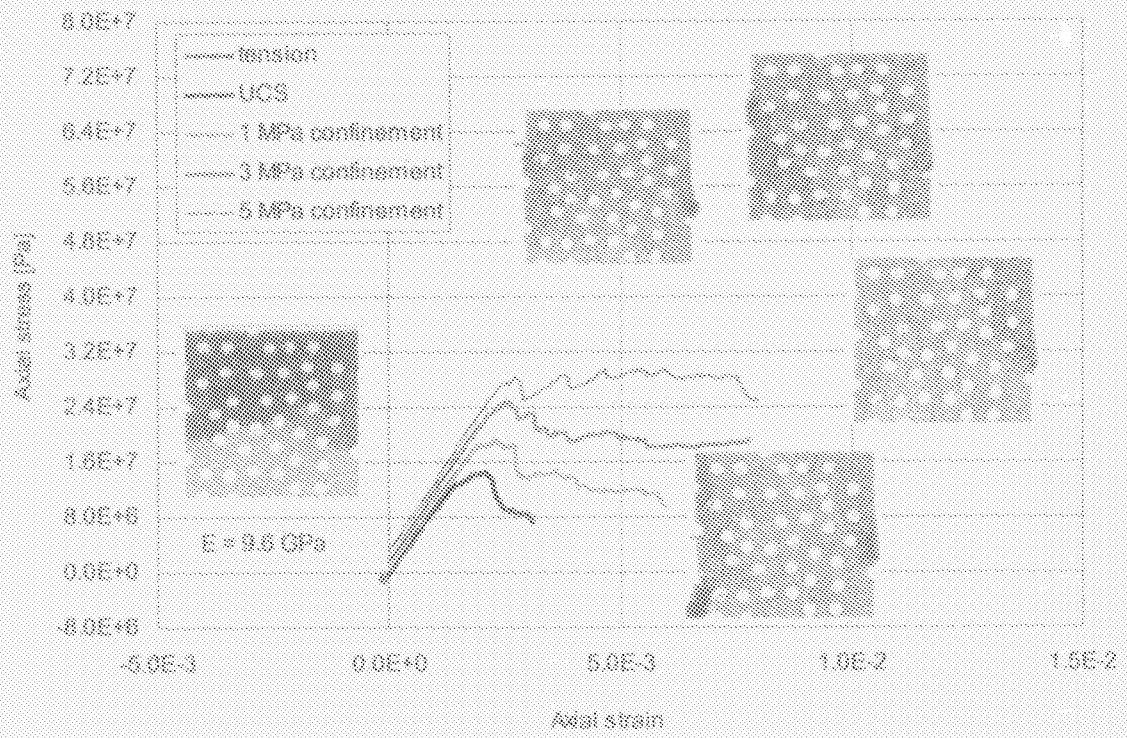

Figure 8 Stress-strain response and failure mechanisms for lithophysal porosity of 23.8% (circular voids distributed randomly throughout the sample)

5.1 Data Reduction

For each sample, histories of the axial stress, axial strain, and volumetric strain were recorded. The history data points were transferred to Excel spreadsheets for post-processing. The Excel spreadsheet contains the raw history data points of axial strain, volumetric strain and axial stress. Based on that raw data, Young's modulus, Poisson's ratio, dilation angle, UCS, internal angle of friction, cohesion, and the Hoek Brown factors σ_{ci} and m_i can be calculated. These quantities were calculated using the following methods.

5.1.1 Peak Compressive Strength

The value of peak compressive strength was taken as the greatest axial compressive stress achieved during the test.

5.1.2 Young's Modulus

Young`s modulus is taken as the ratio of the axial stress to axial strain calculated at a stress equal to 50% of the UCS value (secant method).

5.1.3 Poisson's Ratio

Poisson's ratio (υ) is calculated (at 50% of UCS) using the following formula (which can be derived from elastic theory for plane strain):

$$S_e = \frac{elastic\ \ volumetric\ \ strain}{elastic\ \ axial\ \ strain}$$

$$\upsilon = \frac{1 - S_e}{2 - S_e} \tag{2}$$

5.1.4 Dilation Angle

The dilation angle (ψ) is calculated from the slope of the expansive (plastic) portion of volumetric strain versus axial strain curve. The slope is calculated by a linear fit to the data from the greatest volumetric contraction to the end of the test. The calculation is performed using the internal LINEST function in Excel. The slope then is used to calculate the dilation angle using the following formula:

$$S_p = \frac{plastic\ \ volumetric\ \ strain}{plastic\ \ axial\ \ strain}$$

$$\psi = \arcsin\left(\frac{S_p}{2 + S_p}\right) \times \frac{180}{\pi} \tag{3}$$

5.1.5 Angle of Internal Friction

The angle of internal friction (ϕ) is calculated from the slope of the graph σ_1 vs. σ_3. The slope (S_ϕ) is calculated by a linear fit to the data using the internal trend function in Excel. The peak friction angle is determined using the peak applied compressive stresses. The friction angle is calculated by the following formula:

$$\phi = \arcsin\left(\frac{S_\phi - 1}{S_\phi + 1}\right) \times \frac{180}{\pi} \tag{4}$$

5.1.6 Cohesion

The cohesion (c) is calculated from the friction angle and the UCS using the following formula:

$$c = UCS \times \frac{1 - \sin\phi}{2\cos\phi} \tag{5}$$

5.1.7 Hoek-Brown Failure Parameters

The Hoek-Brown (HB) failure parameters σ_{ci} and m_i were calculated from the triaxial compression test results using the spreadsheet formulated by Hoek (Hoek 1995).

5.2 Summary of Results

The numerical results showing all calculated properties from the uniaxial and triaxial lithophysal tests are presented in Table 2.

The following general observations can be made from the numerical tests:

- reduction of peak compressive strength with increased lithophysal porosity;
- reduction of Young's modulus with increased lithophysal porosity;
- less brittle post-peak response, leading to elastic-plastic response for the higher confining pressures; and
- reduction in tensile strength with increased lithophysal porosity.

The relations of uniaxial compressive strength and Young's modulus to lithophysal porosity are shown in Figures 9 and 10, respectively, indicating good agreement with laboratory compressive strength tests on large diameter (0.27 m to 0.29 m; 10.5 in. to 11.5 in.) core samples of lithophysal tuff from Yucca Mountain. This comparison is important, as it gives confidence that the basic mechanisms give the same trends that are observed in actual tests. This lends added credibility to the results of the triaxial tests for which actual lab-tests results are not available.

The relationship of dilation angle to lithophysal porosity at various confining stresses for lithophysal tuff is shown in Figure 11. It is observed that increasing lithophysal porosity leads to a reduction of dilation angle for all levels of confinement simulated. In addition, the dilation angle is also sensitive to the confinement, and decreases as the confining stress increases.

The *UDEC* peak strength values from the results shown in Figures 6-8 can be used to construct traditional failure envelopes for the lithophysal samples. Figure 12 shows the failure stress values plotted in principal stress space with Hoek-Brown envelopes fit to the results. In each case, multiple simulations were made for each confining stress level in which different random distributions of *UDEC* block structures and void placements were used. The Mohr-Coulomb and Hoek-Brown strength parameters derived from the fits to this data are given in Table 2.

As demonstrated in Figure 12, the primary effect of increasing lithophysal porosity is a significant reduction in the compressive and tensile strength components, with minor strength reduction when the lithophysal porosity is raised above 17.8%. The value of cohesion behaves in a similar way. There is little apparent impact of lithophysal porosity on peak friction angle until porosity exceeds 20%.

Table 2 Physical properties from numerical sample tests on lithophysal tuff

Lith. Porosity (GPa)	Elasticity		Tensile (MPa)	Compressive Strengths				Dilation			Strength		Hoek Brown	
	E	ν		Confining Pressure (MPa)				Confining Pressure (MPa)			ϕ	c (MPa)	σ_{ci} (MPa)	m_i
				0	1	3	5	1	3	5				
0.000	19.8	0.16	4.66	60.1	62.7	69.3	78.7	48°	39°	35°	35°	15.6	59.1	6.2
0.000	19.9	0.16	4.86	59.7	63.4	71.9	78.1	55°	40°	34°	35°	15.4	59.7	6.1
0.000	19.8	0.17	3.91	58.7	62.5	70.5	78.4	49°	42°	36°	37°	14.8	58.4	6.7
0.000	19.8	0.16	4.52	59.9	64.2	72.2	79.0	52°	44°	37°	36°	15.3	60.1	6.3
0.000	19.8	0.16	4.26	55.1	60.1	69.2	76.5	45°	38°	32°	38°	13.3	55.4	7.5
0.103	14.1	0.19	2.11	25.8	30.0	39.5	47.8	42°	32°	27°	39°	6.1	25.2	9.4
0.101	14.3	0.19	1.96	24.4	29.1	33.3	39.8	35°	30°	14°	29°	7.1	24.9	4.6
0.101	14.7	0.18	2.17	28.0	33.0	40.0	48.0	37°	29°	22°	36°	7.1	28.1	7.4
0.101	14.3	0.22	2.16	25.7	32.5	41.4	47.0	38°	30°	29°	38°	6.3	27.0	8.1
0.105	14.1	0.17	2.09	23.8	28.7	34.7	42.3	40°	32°	28°	34°	6.3	23.9	6.7
0.107	13.9	0.18	1.95	21.2	27.0	35.5	40.0	39°	32°	29°	39°	5.0	21.2	9.9
0.103	14.2	0.19	2.09	26.5	29.9	37.0	46.0	37°	38°	25°	36°	6.7	25.6	7.6
0.178	11.0	0.20	1.70	13.7	20.1	26.4	32.0	40°	30°	25°	34°	3.7	15.0	6.9
0.176	11.1	0.19	1.84	16.6	22.6	29.8	35.0	39°	28°	26°	35°	4.4	17.7	7.0
0.171	11.5	0.19	1.74	16.5	22.2	28.9	32.1	35°	29°	25°	31°	4.7	18.1	5.1
0.158	11.8	0.18	1.89	16.0	23.0	31.3	38.7	39°	27°	22°	39°	3.8	16.8	10.3
0.168	11.1	0.19	1.72	15.0	21.4	26.7	31.2	36°	25°	21°	31°	4.3	16.6	5.2
0.173	11.3	0.18	1.62	14.9	20.5	28.5	35.7	34°	27°	21°	37°	3.7	15.1	9.5
0.178	10.6	0.23	1.65	16.0	21.1	28.1	34.6	35°	26°	27°	35°	4.2	16.3	7.4
0.238	9.6	0.21	1.52	14.6	19.4	25.0	29.4	35°	29°	23°	29°	4.3	15.5	4.8
0.254	8.6	0.19	1.46	11.1	15.9	20.9	24.6	35°	19°	13°	27°	3.4	12.2	4.2
0.237	9.7	0.17	1.62	13.2	17.8	24.1	29.0	32°	19°	15°	31°	3.7	13.8	5.8
0.251	9.0	0.18	1.52	13.0	17.0	24.7	29.3	37°	24°	18°	32°	3.6	13.3	6.5
0.240	9.1	0.20	1.55	12.6	17.1	21.7	27.7	30°	27°	18°	29°	3.7	13.0	5.2
0.243	9.2	0.19	1.53	12.5	18.5	23.0	28.0	37°	27°	21°	29°	3.7	13.9	4.9
0.238	9.6	0.19	1.55	15.2	20.0	25.5	28.7	34°	21°	15°	27°	4.7	16.4	3.9

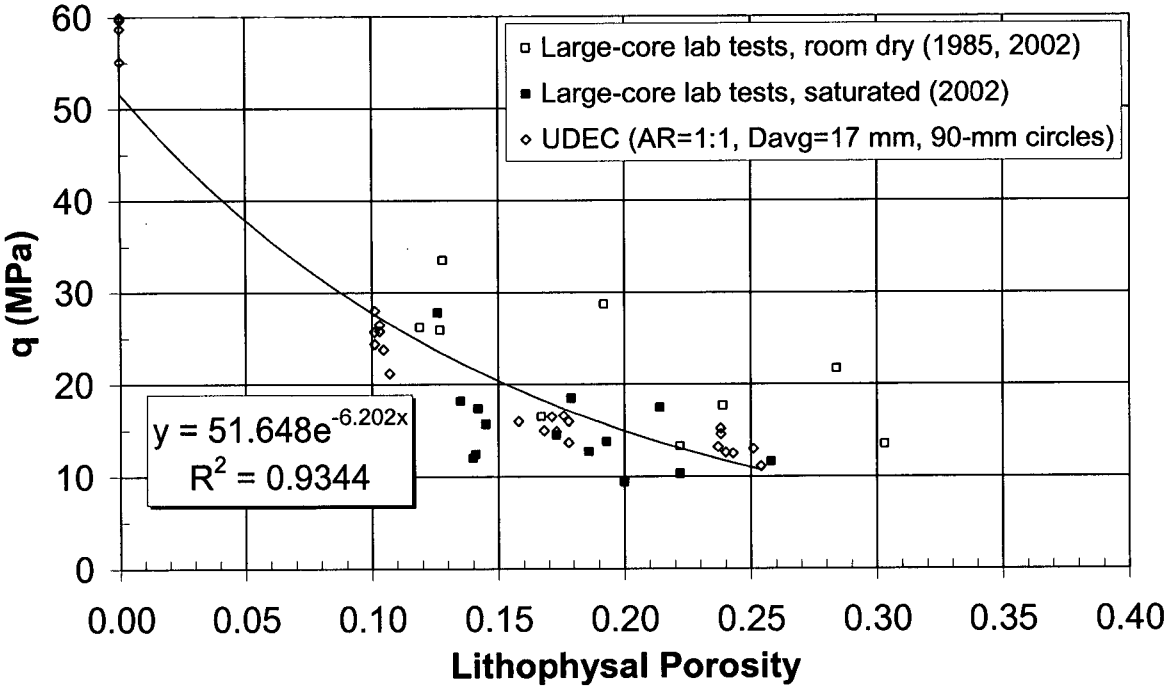

Figure 9. Comparison of *UDEC* simulations of lithophysal porosity effects on uniaxial compressive strength (UCS) to laboratory measurements on large samples.

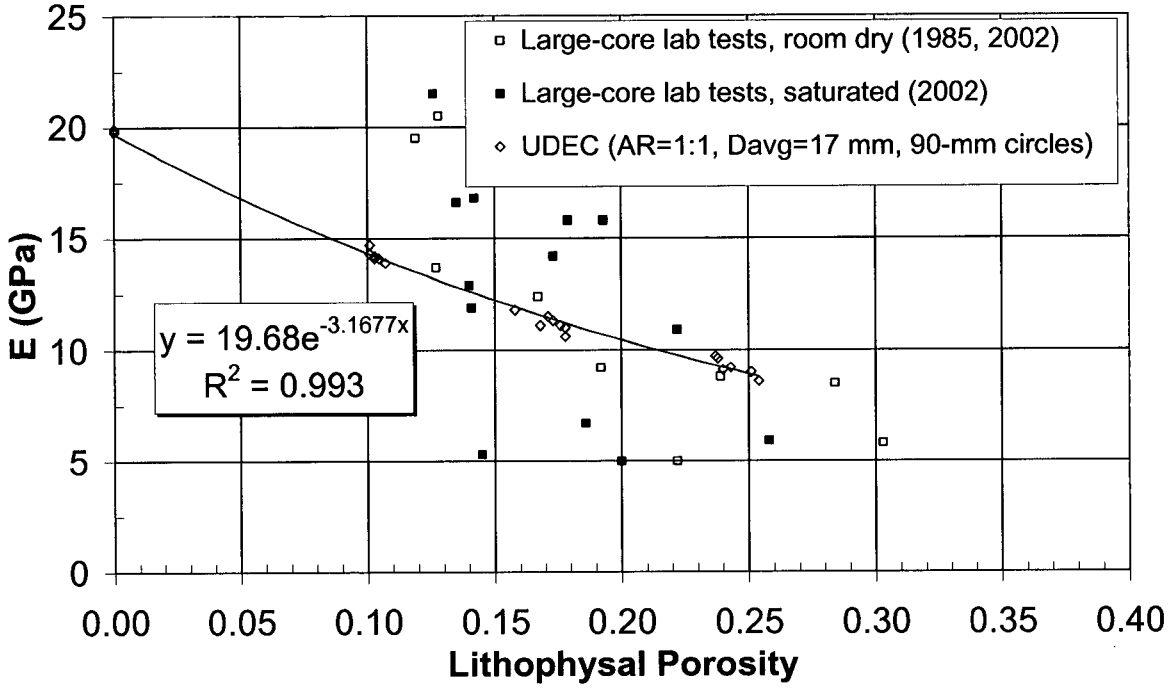

Figure 10. Comparison of *UDEC* simulations of lithophysal porosity effects on Young's modulus to laboratory measurements on large samples.

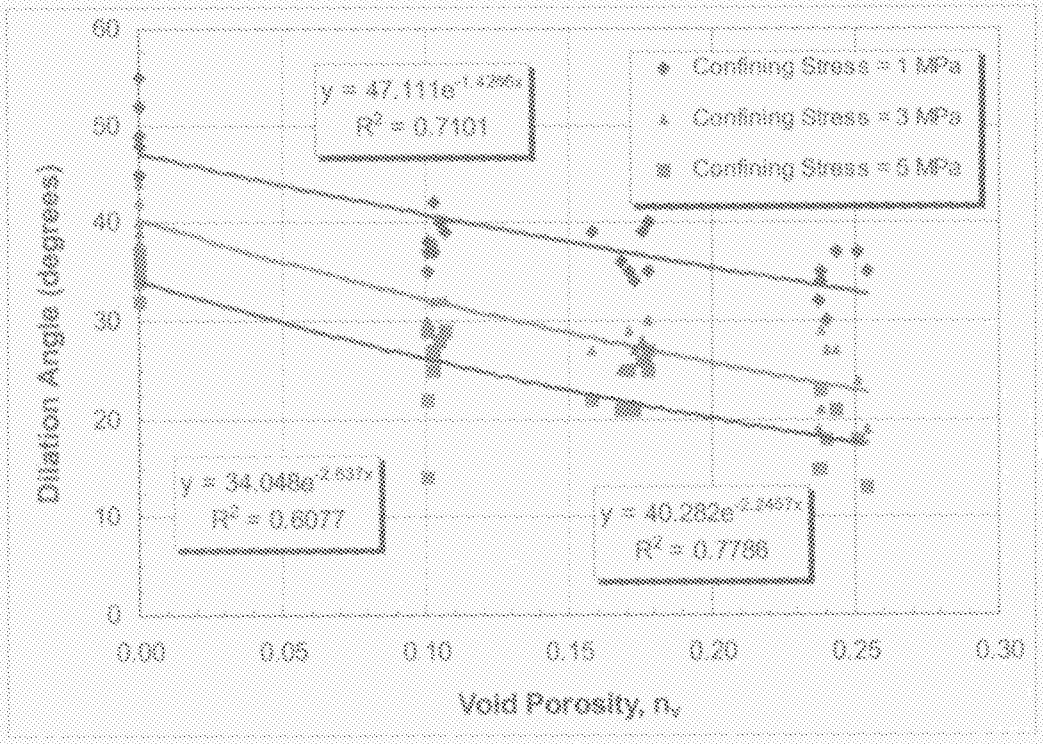

Figure 11. Dilation angles versus lithophysal porosity at various confining stresses from *UDEC* simulations for lithophysal tuff

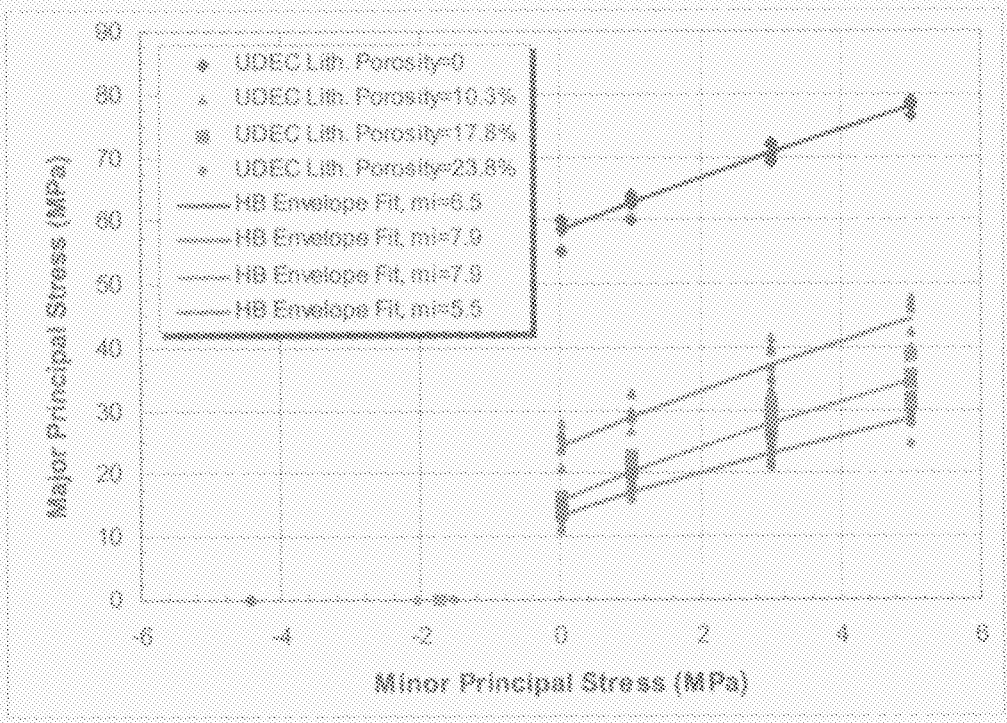

Figure 12. Major principal failure stress versus minor principal failure stress from *UDEC* simulations as well as Hoek-Brown non-linear failure envelope fits for various lithophysal porosities.

6.0 UNCERTAINTIES AND LIMITATIONS IN *UDEC* STUDY

Some uncertainties and limitations are inherent in the current *UDEC* study. These are summarized as follows.

- The effects of lithophysal cavity shape and size on lithophysal rock properties have not been addressed in this study. In the current study, the shape of cavity is circular, and the size is fixed at 0.09 m. In reality, both the shape and the size vary with location. These may be important non-conservative factors that affect lithophysal rock properties and contribute to its behavior.

- The *UDEC* analyses are two-dimensional, whereas the true lithophysal cavities are three-dimensional. The two-dimensional plane-strain models with their infinitely long voids may underestimate strength values, as the third dimension is not available for support and stress redistribution. This aspect of the two-dimensional *UDEC* analyses should be considered conservative.

- The effect of specimen size on lithophysal rock properties has not been addressed in this study. The specimen size of 1 m × 1 m used is small compared to that of a representative volume appropriate for modeling a repository drift. This may or may not affect the derived lithophysal rock modulus and strength properties.

- Pre-existing fractures in the matrix material of lithophysal rock are not accounted for directly by the *UDEC* model. The effect of such fractures may be included in a smeared sense by reducing the contact stiffness and strength between interconnected particles.

- Comparisons of the *UDEC* simulations are made to actual large-core laboratory tests under uniaxial compressive loading conditions only. Though the *UDEC* models were run for triaxial compressive tests, no comparisons have been made due to the lack of actual triaxial test data. To have a greater confidence in the *UDEC* models, use of the data from triaxial compressive tests to validate the models is warranted.

- The current *UDEC* study uses the average large-core laboratory values of Young's modulus and uniaxial compressive strength to calibrate the *UDEC* base-case models and does not account for the effect of variations of rock mass quality or condition. The derived lithophysal properties may be sensitive to these variations. Additional analysis on this sensitivity is considered valuable for further understanding the effect of lithophysal porosity on rock mass properties.

7.0 CONCLUSIONS

The deformational and strength properties of the synthetic lithophysal materials were determined using numerically simulated tensile, uniaxial, and triaxial laboratory tests. Equivalent Mohr-Coulomb and Hoek-Brown yield parameters were determined for the materials. Where possible, the results of these tests were compared with data from actual laboratory tests. This comparison showed that the results of the numerical tests followed the same trends and were bounded by the data from the actual tests.

The general trends noted as specimen lithophysal porosity was increased were:

(a) the peak compressive strength is reduced;

(b) the strength envelope (peak friction angle and cohesion) reduces in size;

(c) the failure response is more ductile; and

(d) the dilation angle decreases.

This study has demonstrated that *UDEC* may be a valuable tool in providing supplemental information for cases where normal laboratory testing data is limited. The derived lithophysal rock properties can be used to supplement limited data collected from laboratory or field testing.

8.0 REFERENCES

Hoek, E., Kaiser, P.K., & Bawden, W.F. 1995. *Support of Underground Excavations in Hard Rock.* Rotterdam: Balkema.

Itasca Consulting Group, Inc. 2002. *UDEC — Universal Distinct Element Code, Version 3.1.* Minneapolis: Itasca.

Potyondy, D. 2002. *Draft of PFC Lithophysal Investigation.* Itasca Consulting Group, Inc. Report, Minneapolis, Minnesota.

Price, R.H.., Nimick, F.B., Connolly, J.R., Kiel, K., Schwartz, B.M., & Spence, S.J. 1985. *Preliminary Characterization of the Petrologic, Bulk, and Mechanical Properties of a Lithophysal Zone Within the Topopah Spring Member of the Paintbrush Tuff.* SAND84-0860. Albuquerque, New Mexico: Sandia National Laboratories. ACC: NNA.19870406.0156.